Second Harmonic Generation characterization of SOI wafers: Impact of layer thickness and interface electric field

D. Damianos, G. Vitrant, M. Lei, J. Changala, A. Kaminski-Cachopo, D. Blanc-Pélissier, S. Cristoloveanu, I. Ionica

Second Harmonic Generation Characterization of SOI Wafers: Impact of Layer Thickness and Interface Electric Field

D. Damianos,[a] G. Vitrant,[a] M. Lei,[b] J. Changala,[b] A. Kaminski-Cachopo,[a] D. Blanc-Pelissier,[c] S. Cristoloveanu[a] and I. Ionica[a]

[a] Univ. Grenoble Alpes, CNRS, Grenoble-INP*, IMEP-LAHC, 3 Parvis Louis Néel – CS 50257, F-38016 Grenoble, France

[b] FemtoMetrix, 1850 East Saint Andrew Place, Santa Ana, CA 92705, USA

[c] INL – UMR 5270, INSA de Lyon, 7 Avenue Jean Capelle, 69621 Villeurbanne, France

Email: dimitrios.damianos@minatec.grenoble-inp.fr

***Abstract* – In this work, we investigate Second Harmonic Generation (SHG) as a non-destructive characterization method for Silicon-On-Insulator (SOI) materials. For thick SOI stacks, the SHG signal is related to the thickness variations of the different layers. However, in thin SOI films, the comparison between measurements and optical modeling suggests a supplementary SHG contribution attributed to the electric fields at the SiO_2/Si interfaces. The impact of the electric field at each interface of the SOI on the SHG is assessed. The SHG technique can be used to evaluate interfacial electric fields and consequently interface charge density in SOI materials.**

Keywords – Second Harmonic Generation; SOI; nonlinear optics modeling; multilayers.

I. INTRODUCTION

The microelectronics industry is in dire need of novel materials in order to overcome the scaling problems of silicon architectures according to ITRS 2013 [1]. State-of-the-art ultrathin Silicon on Insulator (SOI) materials have proven to be excellent alternative candidates for the extension of Moore's law. Before device fabrication though, it is imperative to evaluate the interfacial quality of the material stacks in order to ensure high performance devices and yield. However, the conventional electrical characterization techniques necessitate test device fabrication. Therefore, optical, thus non-destructive characterization techniques, which could potentially be used for in-line, high-throughput wafer inspection, are attractive choices. Among them, the second harmonic generation (SHG) is a nonlinear optical technique based on the second order polarization generated from a material which is shined with a laser light.

*Institute of Engineering Univ. Grenoble Alpes

Centrosymmetric materials such as Si and amorphous SiO_2 do not allow second-order (and generally even-order) order effects such as SHG, due to the presence of an inversion symmetry center [2]. In a material stack like SOI, the second harmonic is generated at different interfaces between Si and SiO_2 [3,4], where the inversion symmetry is broken due to lattice mismatch and the presence of electric fields. It has already been shown [5] that the Si layer thickness can critically impact the SHG response through the absorption of the fundamental and second harmonic (SH) frequencies. Fig. 1 shows the aforementioned impact of the Si film thickness in a SOI structure with a buried oxide (BOX) thickness of 145 nm. This graph was obtained with our homemade simulation tool which will be presented in section III. SHG exhibits a periodic, oscillating behavior with high amplitude variations which depends on the geometry of the SOI stack. Obviously for 6 to 12 inch SOI wafers already in the market, the Si film fluctuations are much smaller than the scale depicted in Fig. 1. Nevertheless, the impact of the film layer thickness on the SHG can be significant. While other techniques are well established for layer thickness measurements, the SHG is now proved to be a very interesting technique for interface characterization, in particular for its ability to probe interface electric fields. More accurate results will need a careful calibration and control of the impact of the film thickness, which is the aim of this paper. It addresses two main points for the SHG behavior from SOI wafers:

a) Optical propagation effects in the SOI multilayer structure.

b) Electric fields at the top and buried interfaces of the SOI structure, and their relevant impact on the SHG response.

In section II, the experimental setup as well as layer thickness and SHG measurements are presented for two different SOI geometries. In section III, the optical simulation, including propagation and absorption phenomena in multilayer systems, is described in detail. The comparison between experimental and modeling results for several SOI stacks in sections IV and V will assess the SHG technique's application for interface characterization.

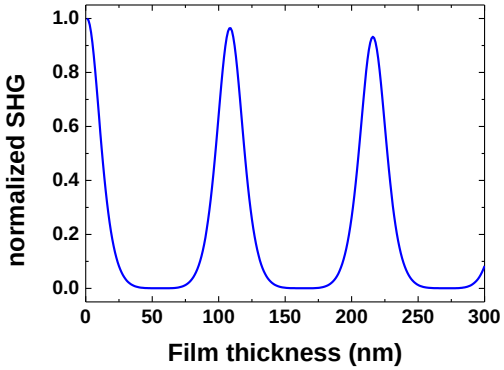

Figure 1: Simulated SHG arising from SOI with varying thickness of the Si film. The thickness used for the BOX was t_{BOX} = 145 nm. The angle of incidence was 45° and the fundamental beam's wavelength was 780 nm.

II. Experimental set-up And SHG Measurements

The SHG measurements were performed with the Harmonic F1X commercial tool from Femtometrix [6] (Fig. 2). A pump laser operating at 780 nm emits femtosecond pulses with 80 MHz repetition rate and 95 fs pulse duration, having an average power of 360 mW and a focused spot diameter of approximately 50 μm on the sample's surface. Along the beam path, a half wave plate is used to control the incident pump polarization. Usually the light is either polarized parallel to the plane of incidence (P-polarization) or perpendicular to the plane of incidence (S-polarization). The high-intensity incident light induces a nonlinear polarization in the sample which generates the second harmonic light at 390 nm, travelling along the reflection angle. The reflected fundamental light is separated from the generated second harmonic (SH) light with the use of proper filters. A rotating polarizer allows the selection of the SH polarization (P or S) for the analysis. Then the SH photons are detected with the help of a photomultiplier tube coupled with a gated photon counter. A reflectometer integrated inside the Harmonic F1X tool allows the measurement of layer thicknesses at the same position on the sample as the SHG. Wafers up to 300 mm in diameter can be tested.

The four SOI structures studied in this paper had different geometries, comprising both thick (145 nm, 88 nm) and thin (24 nm, 12 nm) SOI films. The reflectometry measurements were not accurate enough for the thin Si films. Additionally, the thin film structures (24 nm Si/25 nm BOX and 12 nm Si/145 nm BOX) were small rectangular 5x5 cm coupons instead of whole wafers, so less thickness variation is expected. Subsequently, only the thick structures (145 nm Si/1000 nm BOX and 88 nm Si/145 nm BOX) were used for the thickness variation study.

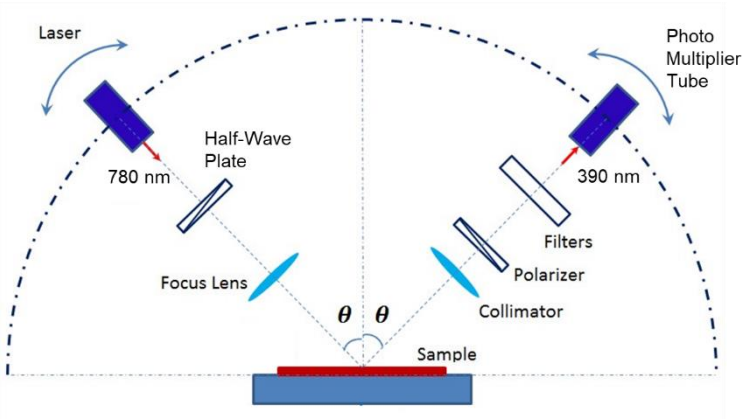

Figure 2: Schematic of the measurement configuration for the SHG system.

In this series of experiments, the Si layer thicknesses and the SH signal were measured on the same spots across different SOI wafers. In Fig. 3a the comparison between Si film thickness and SHG intensity is shown for a thick SOI wafer with t_{Si} = 145 nm and t_{BOX} = 1000 nm (200 mm wafer diameter); a clear correlation is visible for the two quantities. In Fig. 3b the same measurements are shown but for a thinner structure with t_{Si} = 88 nm and t_{BOX} = 145 nm (300 mm wafer diameter). Again, the SHG measurements are clearly correlated with the SOI film variations. However, different trends are obtained for thick and thinner structures. In order to understand this difference, we have developed a tool for simulating optical propagation phenomena in multilayer structures that will be presented in the next section.

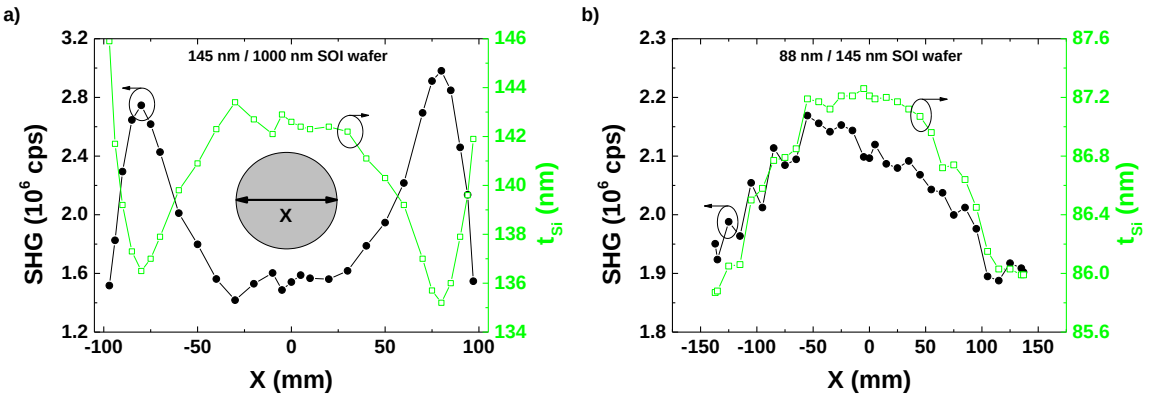

Figure 3: Si film thickness (open squares) and SHG signal (filled circles) for thick (a) and thin (b) SOI wafers. The X-axis in both cases corresponds to different measurement locations on the same wafer, across its diameter (as shown in the inset of Fig. 3a). The angle of incidence was set at 45° and the input / output polarizations at P / P.

III. MULTILAYER OPTICAL MODEL

When light is incident on a multilayer structure the optical phenomena that need to be modelled are: propagation through a layer, absorption inside a medium and transmission at an interface between two media. For this reason the matrix formalism is used [7], which inherently accounts for multiple internal reflections of the radiations inside the stratified media.

The simulated structure, depicted in Fig. 4a, is a system consisting of 5 stacked layers: air, top SiO_2 (native or thermal, if the SOI is passivated), Si film, BOX, Si substrate. The goal is to calculate the optical electromagnetic field at 2ω exiting the structure, $E_{1+}^{2\omega}(0)$, (highlighted with a black circle in Fig. 4c) in order to compare with experiments.

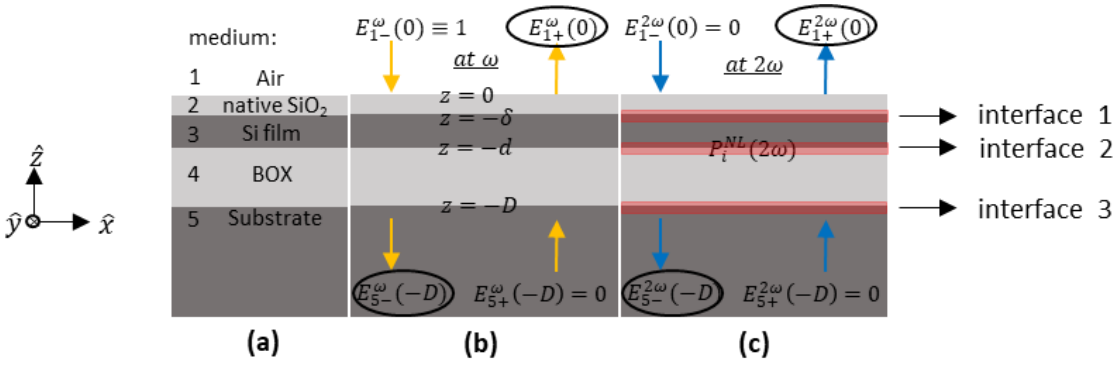

Figure 4: Optical model of the multilayer geometry (a); boundary conditions and calculated fields (circled) for the fundamental frequency (b) and the SH frequency (c). The nonlinear polarization terms are added at each interface, highlighted in (c).

The incident field at the fundamental frequency, $E_{1-}^{\omega}(0)$, is partially reflected, $E_{1+}^{\omega}(0)$, and transmitted, $E_{5-}^{\omega}(-D)$, throughout the entire structure (Fig. 4b). The fundamental electric field will induce the second order polarization of the materials. For centrosymmetric materials like Si and amorphous SiO_2 which possess inversion symmetry and in absence of internal electric fields, 2nd order effects cannot be observed in the bulk. At the interfaces between centrosymmetric media where the inversion symmetry is lift-off, either by the lattice mismatch and/or the dc electric field E_{dc} present, 2nd order phenomena can occur. This second order polarization which drives the SH response is expressed as [3]:

$$P_{2\omega}^{NL} \propto \left| \chi^{(2)} + \chi^{(3)} E_{dc} \right| E_{\omega}^{2} \tag{1}$$

where $\chi^{(2)}$ and $\chi^{(3)}$ are the 2nd and 3rd order susceptibilities, respectively. The extra term depending on the bulk 3rd order susceptibility and a dc field describes the fact that a very small region from the bulk of Si, in the presence of strong electric fields, can create dipolar SH

response. This phenomenon is known as electric field induced second harmonic (EFISH) generation. The static electric field E_{dc} comes from the presence of a space charge region in Si, which is associated with interface traps and fixed oxide charges. This field is mainly localized in the vicinity of Si/dielectric interfaces where it may be very large. "Static" has to be understood as slowly varying compared to the optical frequencies; E_{dc} may thus vary at frequencies up to several tens of GHz while remaining "static" from an optical point of view.

Initially the dc electric field E_{dc} at the interface is not taken into consideration in our simulation, in order to assess whether the optical interferences are the sole contributions to the observed data. For the SHG measurements presented in this paper, where the P-polarized input and P-polarized SH light combination were used, the corresponding theoretical expression for the second order polarization (1.1) becomes [8]:

$$P_{Pp}^{NL} \propto \begin{bmatrix} (\chi_{zxx}^{(2)} \varepsilon_{2\omega} F_s f_c^{\,2} - \chi_{xzx}^{(2)} 2F_c f_s f_c + \chi_{zzz}^{(2)} \varepsilon_{2\omega} F_s f_s^{\,2}) \\ +\gamma F_s + \zeta (3F_c f_c^{\,2} f_s + 4F_s f_s^{\,2} f_c + F_c f_s f_c) \end{bmatrix} E_\omega^2 \qquad (2)$$

with f_s, f_c, F_s, F_c being the Fresnel factors at ω (f_s, f_c) and 2ω (F_s, F_c) which all depend on the angle of incidence θ; $\varepsilon_{2\omega}$ is the dielectric constant of silicon at SH frequency, $\chi_{ijk}^{(2)}$ are the non-zero 2nd order interface susceptibility tensor elements and ζ, γ are bulk quadrupolar susceptibilities whose values were taken from [9]. The polarization in eq. (1) creates SH waves which propagate throughout the structure.

The problem at the fundamental frequency is firstly taken into account. The homogeneous Maxwell equations (with no source terms) are solved and the boundary conditions are taken at each interface [10]. From the boundary conditions, the reflected electric field and the transmitted electric field in the new medium are calculated. The reflected (transmitted) field propagates up (down) to the next interface by a relation of the form:

$$E_{final} = E_{initial} \exp(\pm i k_z d) \qquad (3)$$

where E_{final} is the electric field amplitude right before reflection (transmission), while $E_{initial}$ is the electric field amplitude at the beginning of the layer; d is the thickness of the layer and the plus (minus) sign is chosen for the reflected (transmitted) field. The exponential term which includes the complex wavevector, depends on the complex refractive index of each layer at the specific wavelength, and describes both propagation (real part) and absorption (imaginary part) of the radiation inside the layer. This way the values of the electric fields at each interface can be found.

Next, the fundamental electric fields at each interface are used to calculate the polarization using equation (1.2). This polarization is consequently added as a source term in

the Maxwell's equations and the new boundary conditions are found for the second harmonic fields according to [11]. From these boundary conditions, the transmitted field at 2ω is calculated and, by using the relation (1.3) adjusted for the SH field quantities (wavelength, refractive indices, absorption coefficient), the field is propagated in each layer. The simulation finally gives the electric field at 2ω outside of the structure ($E_{1+}^{2\omega}(0)$, highlighted with a black circle in Fig. 4c) which can be compared with the experimental results.

Additionally, two boundary conditions were used in the simulation:

a) no incident wave at ω and 2ω coming from the medium at the bottom ($E_{5+}^{\omega}(-D)=0$, $E_{5+}^{2\omega}(-D)=0$), due to the fact that physically the radiations both at the fundamental and the SH frequency (absorption depths of ~10 μm and ~70 nm, respectively) are absorbed inside the Si substrate (~775 μm thickness) before they reach the bottom. Hence, there are no reflections caused from the bottom of the substrate (semi-infinite medium).

b) no incident wave at 2ω from the top ($E_{1-}^{2\omega}(0)=0$), since physically the SH light is only generated at the vicinity of each interface.

In the simulation tool the parameters that can be modified are the same as in the experiments: the average power of the fundamental light, the angle of incidence, the thickness and the complex refractive indices (including absorption) of each layer. Furthermore, the values for the susceptibility components and the E_{dc} can be adjusted as well.

Fig. 5a and 5b present the SHG intensity versus the Si film thickness from the measurements (data points from Fig. 2a and 2b) along with the corresponding simulation results (lines), for the two SOI wafers. It should be noted that these simulations were performed with no electric field E_{dc} taken into account. The agreement between simulation (with E_{dc}=0) and experiment is very good, especially for the thick SOI wafer. The correlation for the thinner SOI stack appears less convincing and the data is more dispersed, but the thickness variation is very small (see x-axis in Figure 5b).

Furthermore, it is more difficult to measure ultrathin SOI thicknesses by reflectometry, so another parameter easy to modify experimentally should be used to compare simulation and experiments. This parameter can be the angle of incidence (AOI); its variation alters the path that the light travels inside each medium, effectively changing the SHG response.

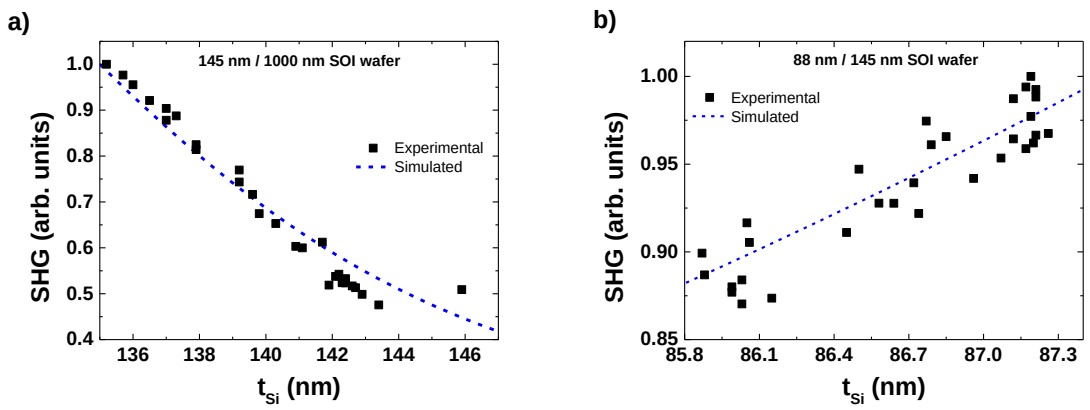

Figure 5: Model (lines) and experiment (data points) comparison of SHG signal versus Si film thickness for thick (a) and thin (b) SOI. The normalized experimental data points were calculated from Fig. 3a and 3b for both cases. The normalization was done by dividing each set (experimental and simulated) by its corresponding maximum value.

IV. SHG VS ANGLE OF INCIDENCE

In this section, SHG experiments were performed for various angles of incidence (AOI) of the fundamental beam. Fig. 6a presents the SHG measurements on the thicker SOI wafer at two locations (with different Si film thicknesses, as measured in Fig. 3a). From Fig. 6b, which shows the calculated SHG, it is evident that by changing only the thickness of the Si film layer in the simulation, the experimental data are fairly well reproduced (shape and peak position).

For thinner SOI with t_{Si} = 88 nm and t_{BOX} = 145 nm (Fig. 7a) the model can reproduce as well the observed behavior (black straight line). This good correlation with the simulation for both geometries (with no dc electric field taken into account) implies that the SHG is mainly given by $\chi^{(2)}$ interface terms. Even if a typical electric field value (10^4 V/cm) is added in the simulation, its impact on the SHG is small and the correlation does not change significantly (red dotted line in Fig. 7a).

The correlation observed on the previous samples is completely lost for thinner SOI substrates: in Fig. 7b the experimental SHG and simulation with no electric field are shifted by more than 20°, for a 24 nm film / 25 nm BOX sample. In a thin film, the model based exclusively on linear optical propagation phenomena appears not sufficient to explain the experimental results. Indeed in thin SOI, the Si/SiO_2 interfaces are coupled together and the electric field can be strong [12]. Hence the vertical dc field (in the z-direction) must be added to the model at every Si/SiO_2 interface by including an extra term $\chi^{(3)}E_{dc}$ in the $\chi_{zzz}^{(2)}$ component in Eq. (1.2), and by using the correct order of magnitude for the $\chi^{(3)}$ value. When using $\chi^{(2)}$ magnitudes from [9] and typical $\chi^{(3)}$ magnitudes from [2], then the ratio of the two quantities

($\chi^{(3)}$ / $\chi^{(2)}$) is of about 10^{-6} m/V. Once $\chi^{(3)}$ is multiplied by E_{dc} (in the order of 10^4 – 10^5 V/cm), their product begins to have the same order of magnitude as the $\chi^{(2)}$.

With the incorporation of a dc field of 10^4 V/cm for the thin SOI with t_{Si} = 88 nm / t_{BOX} = 145 nm (red dotted line in Fig. 7a), and 10^5 V/cm for the ultrathin SOI with t_{Si} = 24 nm / t_{BOX} = 25 nm (green solid line in Fig. 7b), the simulation can better reproduce the observed behaviour. The effect is more prominent for the ultrathin SOI, where a dc field value of 10^4 V/cm (red dotted line in Fig. 7b) is not enough to explain the experimental data.

The aforementioned values are typical at Si/SiO_2 interfaces [13]. The higher E_{dc} value needed for the ultrathin SOI in Fig. 7b is in agreement with the well-known increase of the electric field for decreasing Si film thickness due to coupling between the top SiO_2/Si film and Si film/BOX interfaces [14].

SHG in thicker SOI structures is fairly well simulated by geometry impact on optical propagation and absorption ($\chi^{(2)}$ and layer thicknesses are enough to explain the experimental data). However, for thin SOI the dc electric field must be included in order to better reproduce the data. This is actually a benefit since it confirms the interest in SHG to access the interface electrical fields that are related to the interface quality in SOI. For this application, it is critical to understand the contribution of each interface to the SHG response. In order to do so, in the next section we study the impact that different electric fields at different interfaces can have on the total SHG response.

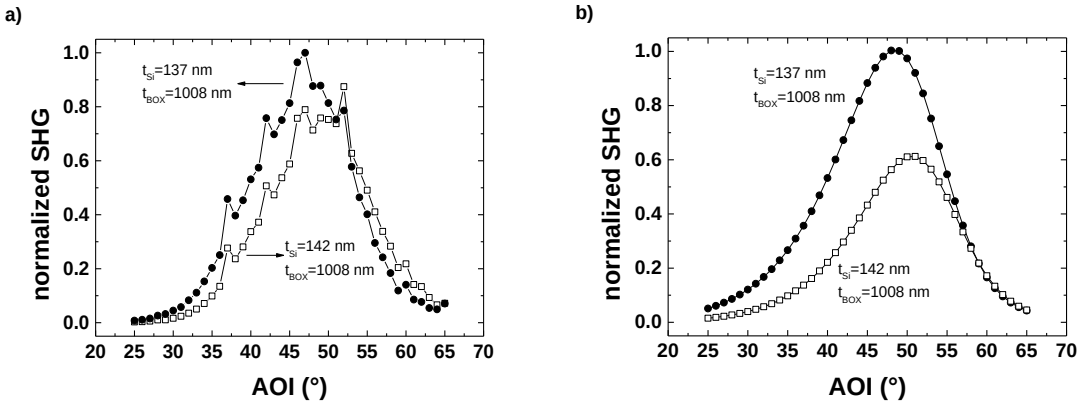

Figure 6: a) Experimental SHG versus angle of incidence (AOI) at two different locations on the same wafer (measured Si layer thicknesses are of 137 nm and 142 nm respectively at each point). b) SHG vs AOI from the simulations obtained with the corresponding Si film thicknesses. The normalization was done by dividing each set (experimental and simulated) by its corresponding maximum value.

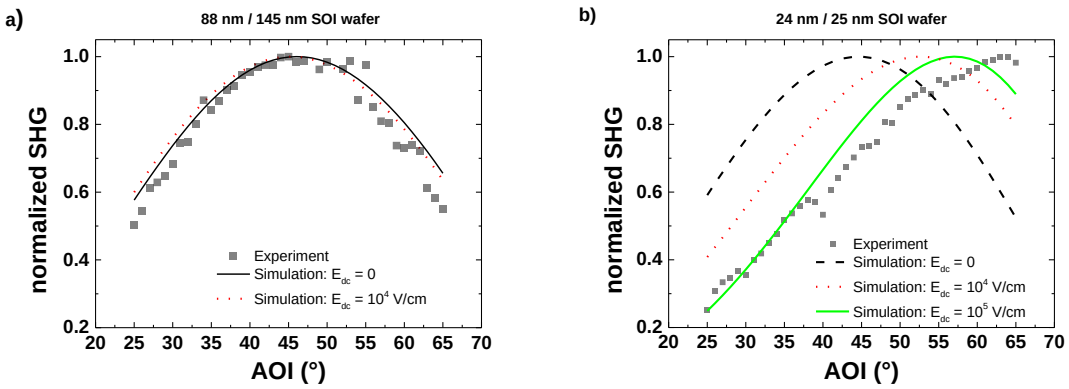

Figure 7: (a) SHG versus angle of incidence (AOI) for the 88 nm / 145 nm SOI. Comparison of experimental data (filled squares) and simulation without E_{dc} (straight black line) as well as with the presence of an electric field E_{dc} = 10^4 V/cm (red dotted line) at all interfaces. (b) SHG versus AOI for an ultrathin SOI structure with 24 nm Si film and 25 nm BOX thicknesses. The value of the electric field included at all interfaces in the simulation was E_{dc} = 10^4 V/cm (red dotted line) and E_{dc} = 10^5 V/cm (green solid line).

V. Impact of The Interfacial DC Fields

In SOI stacks the different interfaces do not always have the same properties, i.e. interface state density and trapped charge [15]. Therefore, the strength of the dc electric field at the top and buried interfaces will be different, hence the generated second order polarization will be interface dependent and the global SHG response will vary.

It is important to note that the escape depth of the fundamental light (at 780 nm) is 10 µm while the one for the SH light (at 390 nm) is 70 nm. These values were calculated by the inverse of the absorption coefficient of Si at 300 K (1030 cm^{-1} at 780 nm and 1.43e5 cm^{-1} at 390 nm) taken from [16]. This means that for Si films with thicknesses higher than 70 nm, only the very top interface (top SiO_2 / Si film) contributes to the SH signal at 390nm wavelength. For much thinner films, the buried interfaces (Si film / BOX, and BOX / Si substrate) will influence the SH response as well. The BOX is transparent to 390 nm light, so even the SH from the very bottom interface (BOX / Si substrate) might have an impact. In order to investigate where the dominant contribution comes from, simulations were made with different electric fields independently varied at each interface (only one is varying while the others are kept zero).

Primarily the thicker 88 nm / 145 nm passivated SOI was investigated. As it is observed in Fig. 8a, the change of the E_{dc} value at the top interface (SiO_2 / Si film) influences the simulated SH signal. It is visible that as the electric field increases, the peak of the AOI curves shifts to lower angles. For more quantitative comparisons between the experimental and

simulated curves, the relative positions of the AOI peaks are calculated. Specifically, θ_{exp} is the position of maximum (peak) in the experimental data while $\theta_{simulated}$ is the position of maximum in the simulated data. Figure 8b shows the relative position versus the electric field value at the top interface. The straight line at y=0 gives the value of the E_{dc} field for which the simulated and experimental AOI peaks coincide, and it is the point of reference which is used for comparison. The best match here is achieved for a field of 10^4 V/cm. This relatively small value for the electric field is supported by the fact that the sample had a passivated Si film.

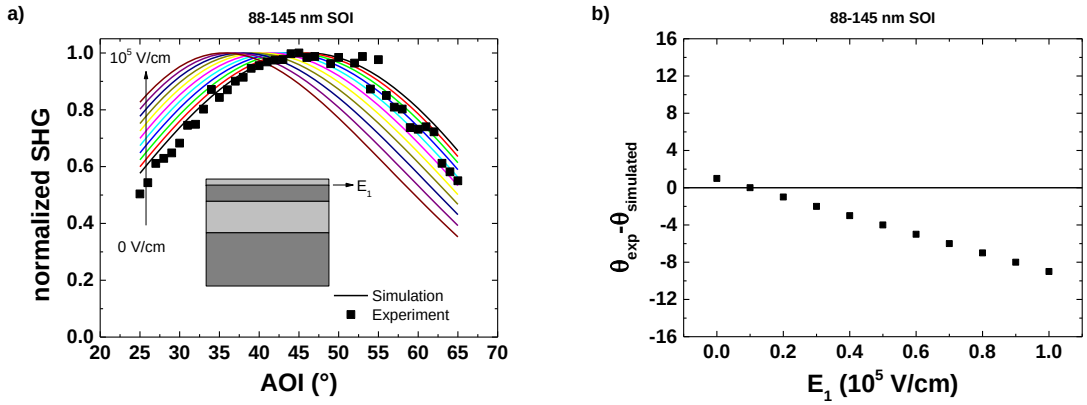

Figure 8: a) Variable E_1 field for the thicker SOI structure (t_{Si} = 88 nm / t_{BOX} = 145 nm). b) Difference between experimental and simulated AOI peak position (θ_{exp}, $\theta_{simulated}$ respectively) versus the static electric field at the first interface, between the passivated layer and the Si film.

In thinner SOI structures we expect that the influence of E_{dc} at the bottom interfaces might also play a role in the SHG behavior. In Fig. 9 the influence of the dc electric field for the thin 12 nm / 145 nm SOI structure is depicted. Specifically, Fig. 9a shows the impact of varying only the very top field (E_1) at the top SiO_2 / Si film interface, while the other two fields were neglected (E_2=E_3=0). From Fig. 9b the best match is achieved when the top field has a value of ~9x10^4 V/cm. This E_{dc} value is higher than the one needed for the simulation of the thicker SOI, which is consistent with the fact the thinner Si film couples more efficiently the top and buried interfaces [14].

Correspondingly, Fig. 9c and 9d show the results for varying only the middle field (E_2), at the Si film / BOX interface, while the others were kept at zero (E_1=E_3=0). A relatively small variation of the simulated SHG curve is evidenced, but it is less significant compared to the previous case. The position of the peak is modified by the electric field at the film/BOX interface, but it cannot be adjusted to fit the experiments because E_1=0, which is not realistic.

Last, Fig. 9e and 9f present the effect of varying only the bottom field (E_3), at the buried BOX / Si substrate interface, while keeping the others zero (E_1=E_2=0). The variation between

the curves simulated with different E_3 values is hardly visible and the position of the simulated peak is practically constant. The absence of match between experimental and simulated peaks confirms that the 3rd interface (buried) has no influence on the SHG measured on such samples. When comparing all curves together (Fig. 9a, 9c, 9e) it is clear that the top interfacial field plays the most critical role; this stems from the fact that the SH generated at the buried interfaces is partially absorbed as it travels through the 12 nm Si film. This does not necessarily mean that the dc field is higher there, but that the SHG is most sensitive to the changes at the very top interface.

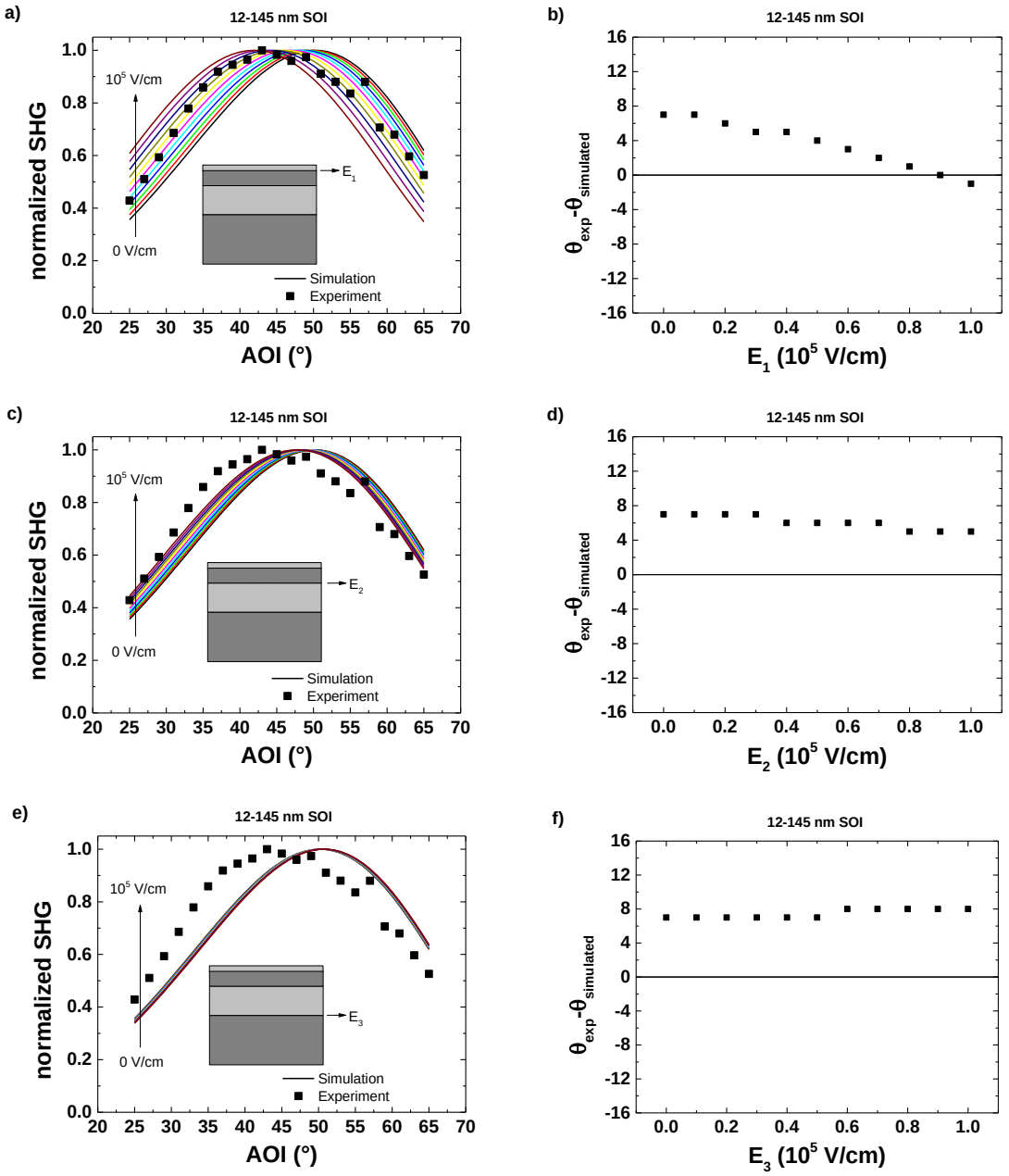

Figure 9: Simulated 12 nm / 145 nm SOI structure with different values of dc electric field at the different interfaces: a) E_1 variable, E_2=E_3=0, b) E_2 variable, E_1=E_3=0, b) E_3 variable, E_1=E_2=0.

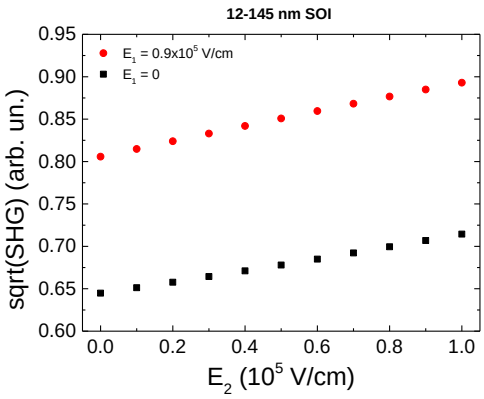

Figure 10: Simulated square root of SHG signal from a 12 nm / 145 nm SOI structure versus the electric field at the buried interface E_2, for two different values of the electric field at the top interface, E_1=0 and E_1=0.9x10^5 V/cm (this value was taken from Fig. 9b, since it is the best match to the maximum AOI). The square root of the SHG signal is preferably used here since it is directly proportional to the value of the electric field E_{dc}, according to eq. (1).

Indeed, the influence of the buried interfaces is smaller, since the SHG generated from them is partially absorbed from the Si film. Nevertheless, the reflected SHG signals contain this small information.

A way to probe the buried interfaces would be, for example, "fixing" a value of the electric field at the top interface, which is prominent, and tune the value of the field from the buried interface. Fig. 10 shows the simulated SHG versus the electric field E_2 (buried interface) for two different values of the electric field E_1 (top interface). We observe that for both E_1 values, the SHG signal varies significantly as we change the value of E_2. From a pragmatic point of view this means that if we have SOI structures with the same passivation (E_1 fixed), the fabrication variants that impact the buried interface will be significantly measurable with SHG.

VI. Conclusion

In this work, the SH signal generated from various SOI wafers was correlated with the Si film thickness. This interdependence was established for thick SOI structures and verified by a home-made simulation tool. This tool uses an optical multilayer model which takes into account the nonlinear polarization at each interface. For the thinner SOI, absorption and optical interferences are not enough to reproduce the experimental behavior. Thus, a supplementary term related to the dc electric field at each interface was added in the simulation in order to

better explain the corresponding data. The simulation demonstrated that SHG is sensitive to the changes in the dc electric fields, the most prominent being the one from the top interface. Far from being a drawback, this implies that the SHG technique corrected for thickness variations can be an excellent tool to access information about the interfacial electric fields (E_{dc}), leading to characterization of interface states (Q_{ox} and D_{it}) and quality control in SOI wafers.

ACKNOWLEDGMENT

This work is supported by Region Rhône Alpes (ARC6 program). We would also like to thank SOITEC for providing some of the wafers and for inspiring discussions.

REFERENCES

[1] ITRS 2013, http://www.itrs2.net/2013-itrs.html.

[2] R. W. Boyd, "Nonlinear Optics", 3rd edition, Elsevier, 2008.

[3] B. Jun *et al.*, *Appl. Phys. Lett.*, vol. 85, no. 15, pp. 3095–3097, 2004.

[4] M. L. Alles *et al.*, *IEEE Trans. Semicond. Manuf.*, vol. 20, no. 2, pp. 107–112, 2007.

[5] D. Damianos *et al.*, *Solid. State. Electron.*, vol. 115, pp. 237–243, 2016.

[6] www.femtometrix.com.

[7] O. S. Heavens, *Optical properties of thin solid films*. Courier Corporation, 1965.

[8] J. E. Sipe, D. J. Moss, and H. M. Vandriel, *Phys. Rev. B*, vol. 35, no. 3, pp. 1129–1141, 1987.

[9] Y. Q. An, R. Carriles, and M. C. Downer, *Phys. Rev. B*, vol. 75, no. 24, p. 241307, 2007.

[10] J. D. Jackson, *Classical Electrodynamics*. John Wiley & Sons, 2007.

[11] J. A. Armstrong, N. Bloembergen, J. Ducuing, and A. P. S. Pershan, *Phys. Rev.* vol. 127, no. 6, 1962

[12] G. Hamaide, F. Allibert, H. Hovel, S. Cristoloveanu, and S. S. Li, *J. Appl. Phys*, vol. 101, pp. 114513–317, 2007.

[13] N. Shamir, J. G. Mihaychuk, and H. M. van Driel, *J. Appl. Phys.*, vol. 88, no. 2, p. 896, 2000.

[14] G. Hamaide, F. Allibert, F. Andrieu, K. Romanjek, and S. Cristoloveanu, *Solid State Electron.*, vol. 57, pp. 83–86, 2011.

[15] A. Toriumi, J. Koga, H. Satake, and A. Ohata, *Proceedings of International Electron Devices Meeting*, pp. 847–850, 1995.

[16] M. A. Green, *Solar Energy Materials and Solar Cells*, vol. 92, pp. 1305-1310, 2008.